Fermi National Accelerator Laboratory

FERMILAB-Pub-91/213-E

Study of the χ_1 and χ_2 Charmonium States Formed in $\bar{p}p$ Annihilations

The E760 Collaboration
Fermi National Accelerator Laboratory
P.O. Box 500, Batavia, Illinois 60510

August 1991

* Submitted to *Nuclear Physics B*.

Study of the χ_1 and χ_2 Charmonium States Formed in $\bar{p}p$ Annihilations

T.A. Armstrong[6], D. Bettoni[2], V. Bharadwaj[1], C. Biino[7], G. Borreani[2], D.R. Broemmelsiek[4], A. Buzzo[3], R. Calabrese[2], A. Ceccucci[7], R. Cester[7], M.D. Church[1], P. Dalpiaz[2], P.F. Dalpiaz[2], M. Dameri[3], D. Dimitroyannis[5], M. Fabbri[2], J.E. Fast[4], S. Ferroni[3], M. Gee[4], C.M. Ginsburg[5], K.E. Gollwitzer[4], A.A. Hahn[1], M.A. Hasan[6], S.Y. Hsueh[1], R.A. Lewis[6], E. Luppi[2], M. Macrí[3], A.M. Majewska[6], M.A. Mandelkern[4], F. Marchetto[7], M. Marinelli[3], J.L. Marques[4], W. Marsh[1], M. Martini[2], M. Masuzawa[5], E. Menichetti[7], A. Migliori[7], R. Mussa[7], S. Palestini[7], N. Pastrone[7], C. Patrignani[3], J. Peoples Jr.[1], L. Pesando[7], F. Petrucci[2], M.G. Pia[3], S. Pordes[1], P.A. Rapidis[1], R.E. Ray[5,1], J.D. Reid[6], G. Rinaudo[7], J.L. Rosen[5], A. Santroni[3], M. Sarmiento[5], M. Savrié[2], J. Schultz[4], K.K. Seth[5], G.A. Smith[6], L. Tecchio[7], S. Tommasini[3], S. Trokenheim[5], M.F. Weber[4], S.J. Werkema[1], Y. Zhang[6], J.L. Zhao[5], G. Zioulas[4], M. Zito[3,a].

[1] *Fermi National Accelerator Laboratory, Batavia, Illinois 60510, U.S.A.*

[2] *I.N.F.N. and University of Ferrara, 44100 Ferrara, Italy*

[3] *I.N.F.N. and University of Genoa, 16146 Genoa, Italy*

[4] *University of California at Irvine, California 92717, U.S.A.*

[5] *Northwestern University, Evanston, Illinois 60201, U.S.A.*

[6] *Pennsylvania State University, University Park, Pennsylvania 16802, U.S.A.*

[7] *I.N.F.N. and University of Turin, 10125 Turin, Italy.*

To be submitted to Nuclear Physics B

[a] *Now at CEN-Saclay, F-91191 Gif sur Yvette, France*

P.A.C.S. numbers 13.75 Cs, 14.40Jz

Abstract

We report on a study of the $\chi_1(^3P_1)$ and $\chi_2(^3P_2)$ states of charmonium formed in antiproton–proton annihilations. An energy scan through the resonances, performed with a very narrow momentum–band beam of antiprotons intersecting a hydrogen jet target, enables us to perform very precise measurements of the mass and the total width of the two resonances.

From a sample of 513 χ_1 and 585 χ_2 events we find:

$M_{\chi_1} = (3510.53 \pm 0.13)$ MeV/c^2 ; $M_{\chi_2} = (3556.15 \pm 0.14)$ MeV/c^2 ;

$\Gamma_{\chi_1} = (0.88 \pm 0.14)$ MeV ; $\Gamma_{\chi_2} = (1.98 \pm 0.18)$ MeV ;

From our measurement of the quantity $\Gamma(R \to \bar{p}p) \times BR(R \to J/\psi\gamma) \times BR(J/\psi \to e^+e^-)$, using known branching ratios, we obtain: $\Gamma(\chi_1 \to \bar{p}p) = (69 \pm 13)$ eV ; $\Gamma(\chi_2 \to \bar{p}p) = (180 \pm 31)$ eV

1. Introduction

In this paper we report results from the first run of Fermilab experiment E760 devoted to a systematic study of charmonium states formed in the process:

$$\bar{p} + p \to (\bar{c}c). \tag{1.1}$$

Antiprotons stored in the Fermilab Accumulator collide with the protons of a continuously flowing internal molecular hydrogen jet target. With this arrangement, which efficiently uses the circulating antiprotons, we obtain a high luminosity ($\sim 10^{31}$ cm^{-2} s^{-1}), small size interaction source. The target thickness traversed by particles at each turn is $\sim 10^{-10}$ g cm^{-2}.

In this experiment the spread of the center of mass energy ($W = \sqrt{s}$) is approximately

$\Delta W \sim 250$ keV*, a value which is 3 to 4 times smaller than the one achieved in a previous experiment at the CERN ISR, which successfully pioneered this technique[1] This value allows for the direct measurement of resonance widths in the sub–MeV region [2].

We report here the first measurement of the total width of the $\chi_1(^3P_1)$ state of charmonium and new precise measurements of the $\chi_2(^3P_2)$ total width and of the masses and partial widths to $\bar{p}p$ for both resonances. These quantities constrain the QCD theory parameters and the features of the phenomenological models that have been used to describe charmonium [3] and may provide clues to a better understanding of quark–antiquark interactions in this energy regime.

2. Experimental Technique

The Breit–Wigner resonant cross section for reaction (1.1), summing over all $(\bar{c}c)$ decay channels, is:

$$\sigma = \frac{4\pi(\hbar c)^2}{(W^2 - 4m^2c^4)} \times \frac{(2J_R+1)}{(2S+1)\times(2S+1)} \times \frac{\Gamma(R \to \bar{p}p)\Gamma_R}{\left[(W - M_R c^2)^2 + \Gamma_R^2/4\right]}; \qquad (2.1)$$

where S, m are the proton spin and mass, J_R, M_R, Γ_R are the resonance parameters and $\Gamma(R \to \bar{p}p)$ is the partial width of the resonance to the $\bar{p}p$ state. For the χ_1 and χ_2 states, the formation cross section is about 10^6 times smaller than the hadronic non–resonant $\bar{p}p$ total cross section in this energy region, which makes it impractical to extract a signal searching for the hadronic decay modes of the χ's. An almost background–free sample can be selected, however, if we limit the search to the radiative decay channels and study the formation–decay process:

$$\bar{p} + p \to \chi \to J/\psi + \gamma \to e^+ + e^- + \gamma \qquad (2.2)$$

*All the quoted errors represent the r.m.s. of the distributions.

which at $W = M_R c^2$ has a cross section $\sigma_{peak} \sim 2$ nb.

The parameters of the resonance are extracted from the excitation curve, that is, from a measurement of the cross section for reaction (2.2) versus the center of mass energy in the resonance region. The excitation curve is the convolution of the resonance profile and of the center of mass energy distribution function. When the resonance natural width is comparable to or smaller than the energy distribution width, an accurate knowledge of the latter becomes an essential ingredient to properly perform the unfolding of the intrinsic resonance width from the measured excitation profile.

In the experimental arrangement of E760, where an antiproton beam collides with an effectively stationary target, the center of mass energy depends only on the beam energy through the equation $W^2 = 2mc^2(E_{beam} + mc^2)$.

Two pieces of information are then essential: the absolute scale of the beam energy to correctly determine the mass of the state and the beam momentum spectrum to extract the width of the resonance.

The absolute energy scale has been determined by performing an energy scan at the J/ψ and ψ' resonances[4]. The masses of both resonances are known to $\Delta M_R \simeq 100$ keV/c^2 [5]. At the resonance peak we obtain (neglecting the small statistical uncertainty in the experimental determination of the peak location):

$$\Delta W = \Delta M_R c^2 \quad \text{and} \quad \Delta E_{beam} = (M_R/m)\, \Delta M_R c^2. \tag{2.3}$$

The beam energy can also be written in terms of the antiproton revolution frequency in the accumulator f_r and of the length of the orbit L_{orb} as:

$$E_{beam} = mc^2/\sqrt{(1-\beta^2)} = mc^2/\sqrt{\left[1-(f_r L_{orb}/c)^2\right]} \tag{2.4}$$

and the error on the beam energy as:

$$\Delta E_{beam} = mc^2\,(\gamma_{beam})^3\,(\beta_{beam})^2\left[(\Delta f_r/f_r)^2 + (\Delta L_{orb}/L_{orb})^2\right]^{1/2}. \tag{2.5}$$

Since the revolution frequency is measured very precisely ($\Delta f_r/f_r \sim 2 \times 10^{-7}$), the uncertainty ΔM_R translates into an uncertainty in the length of the orbit by $\pm$ 2 mm at the J/ψ and by $\pm$ 0.7 mm at the ψ'.

The distribution function of the beam revolution frequency, f_r, is derived from an analysis of the beam current Schottky noise spectrum. The shape of the beam momentum (p) spectrum can then be obtained if one knows the factor $\eta = (\delta f_r/f_r)/(\delta p/p)$, where $\eta = m^2c^4(E_{beam}^{-2} - E_T^{-2})$ depends on the value of the Antiproton Accumulator transition energy E_T. We exploited different techniques[4] to measure the value of η and estimate an error on its determination of $\sim \pm 10\%$.

To achieve reasonable rates for events with a cross section of a few nanobarns, one needs a high luminosity source and a large acceptance detector. Peak luminosities of $\sim 8 \times 10^{30}$ cm^{-2} s^{-1} were achieved with a beam of 2.5×10^{11} antiprotons circulating in the accumulator ring and traversing, at a frequency of $\sim$ 0.63 MHz, an internal H_2 jet target of $\sim 5 \times 10^{13}$ atoms/cm^2. The target is similar in design and performance to the one used in the ISR experiment[1,6]. A useful feature of this experimental arrangement is the small size of the interaction region which is defined transversely by the dimension of the beam ($r_{beam} \sim 3.5$ mm for 95% containment) and longitudinally by the thickness of the H_2 jet ($\sim$ 8 mm).

A typical data taking cycle lasted about 90 hours, including 40 hours of antiproton accumulation at an average rate of $\sim 0.5 \times 10^{10}$ $\bar{p}$ per hour. Once the accumulation process was complete, the beam was stochastically cooled and decelerated to an energy slightly above the resonance region. The beam was then decelerated in small momentum steps (between 200 and 500 keV/c) and data collected at several points across the resonance. The data taking lasted typically 50 hours corresponding to an integrated luminosity of the order of 500 nb^{-1}. In 10 weeks during the summer of 1990, we collected data for an integrated luminosity of 5.9 pb^{-1}. A summary of the data recorded is given in Table 1.

3. The Detector

The detector (Figure 1) is a non–magnetic spectrometer with cylindrical symmetry and full azimuthal coverage, consisting of a central region (barrel) with polar angle acceptance ranging from 12^0 to 70^0, and an instrumented forward end–cap extending the acceptance down to 2^0. It is optimized for the detection of $e^+e^-, e^+e^-\ \gamma$ and $\gamma\gamma$ high mass final states and for the suppression of the hadronic background simulating these electromagnetic decay channels.

An array of silicon detectors, viewing the interaction region from a distance of ~ 1.5 meters and covering an angle from 82^0 to 90^0 relative to the beam direction, measure the direction and energy of the recoil proton from forward antiproton elastic scattering and allow for the determination of the elastic cross–section parameters down to the Coulomb region. Measurement of the rate of elastic scattering during data taking provides a continuous, absolute and precise monitor of the luminosity [7].

The central detector has been made extremely compact in order to fit in the limited space available inside the Accumulator tunnel. It is built of a sequence of cylindrical layers surrounding the vacuum pipe of the Accumulator; from the beam line out: a) a scintillator hodoscope with 8–fold azimuthal segmentation (H1), b) a straw–tube drift chamber made of two layers of aluminized mylar tubes, with charge–division read out to also measure the coordinate along the beam direction [8], c) a radial projection chamber which samples up to 16 ionization measurements along charged tracks and d), supported by the same mechanical structure, a MWPC with transverse pad readout to improve the measurement of the longitudinal coordinate[9], e) a second hodoscope (H2) with 32 elements followed by f) a threshold Cherenkov counter ($\check{C}$) with an 8–fold azimuthal, 2–fold polar segmentation ($15^0 < \theta < 38^0$ and $38^0 < \theta < 65^0$)[10], g) a set of external tracking elements[11] consisting of a cylindrical barrel of two layers of Iarocci tubes and of a planar multiwire proportional chamber in the forward direction, extending the acceptance down to 12^0 and, finally, h)

an electromagnetic calorimeter built from 1280 lead glass towers pointing to the interaction source, arranged in 20 'rings' and 64 'wedges'[12].

The barrel detector is complemented by a forward end–cap with three elements: a scintillator counter with 8–fold azimuthal segmentation and a planar straw chamber backed by a fine sampling Pb/scintillator calorimeter built from towers individually read out through wavelength–shifter bars[13].

The signal from each photomultiplier of the different detectors is sent to an 11–bit FERA ADC. In parallel, the signals from H1, H2 and the Cherenkov are also sent to digital latches, while the signals from the calorimeter's elements are summed with fast circuitry into a reduced number of analog outputs (6 for the forward calorimeter and 40 for the central one). The 40 signals from the lead glass counters are arranged into a 5 x 8 matrix, mapping the central calorimeter with a coarse θ/ϕ energy grid.

Since a detailed description of all the detector elements can be found in the literature, here we only summarize their performance. The angular resolution achieved with the tracking system is 4 mrad in polar angle (θ) and 7 mrad in azimuth (ϕ) . The energy resolution for the central calorimeter is $\Delta E/E = 0.06/\sqrt{E(\mathrm{GeV})}$, while that for the forward calorimeter is $\Delta E/E = 0.11/\sqrt{E(\mathrm{GeV})}$. The combination of a small source size and good calorimeter granularity yields a precision in the measured direction of photons comparable to that for charged particles (6 mrad in θ and 8 mrad in ϕ).

With this detector we achieved an adequate electron/hadron separation. In particular, using the information from the Cherenkov counters coupled to the information from the calorimeter we succeeded in suppressing the $\pi^{\pm}$ punch–through component to a very low level (≤ 1 out of 10^3 hadrons simulated a high energy electron)[10].

4. Trigger and Event Selection

The final state of reaction (2.2) has a simple topological structure: 2 high $p_\perp$ $e^\pm$ and a photon pointing back to the interaction region. The J/ψ carries a large fraction of the antiproton momentum and, consequently, the two–body correlation between the kinematical variables of e^+ and e^- is only slightly smeared in the laboratory system and the e^+e^- and $\bar{p}$ momentum vectors are nearly coplanar. We used a trigger that selected events with both e^+ and e^- in the barrel volume. In the analysis we further restricted the fiducial region to accept only events with both e^+ and e^- with polar angle $15^0 < \theta < 60^0$. If the γ was emitted with polar angle $2^0 < \theta < 70^0$ it was detected by the calorimeter system.

At the fast trigger level, we designed a logic with loose constraints to select a high mass object decaying to e^+e^-. The essential elements entering the trigger were: logic signals from the Cherenkov cells and from the scintillator hodoscopes (H1 and H2) and the matrix of 5 x 8 analog sums from the lead glass counters. The trigger required that a Cherenkov signal be associated with each of two charged tracks originating from the interaction region, as defined by an appropriate coincidence between the elements of the H1 and H2 hodoscopes. Independently we required two clusters in the central calorimeter separated by more than 90^0 in azimuth and with energy above a threshold, which depended on the polar angle. The number of accompanying charged particles was only limited by the requirement of ≤ 4 hits in each of the two hodoscopes (H1 and H2). This trigger scheme selected efficiently all $(\bar{c}c)$ resonances decaying either inclusively to a J/ψ or exclusively to e^+e^-. Two additional triggers were implemented on the complete sample of data to monitor the efficiency of the Cherenkov and of the lead glass trigger components: the first one relaxed the condition that both charged tracks be tagged as an electron by the Cherenkov while the second one did not require signals from the central calorimeter. In both cases, to keep the rate to a reasonable level, only events with charged particle multiplicity of 2 and the two tracks nearly coplanar ($|\phi_1 - \phi_2| > 163^0$) were accepted. The data were read from CAMAC using the Fermilab Smart Crate Controller [14] and ACP system [15]. The overall rate was ≤ 10 Hz and all

the events selected by the fast triggers could be recorded on tape without introducing a significant dead time.

Two independent analysis chains were carried out in order to extract a clean event sample. A preliminary selection, common to both analysis chains, required the association of the two largest central calorimeter clusters to charged tracks (electron candidates), at least one of them tagged as an electron by a signal from the corresponding Cherenkov cell. For all events satisfying these requirements, the invariant mass for the two electron system was calculated as $m_{ee}c^2 = \sqrt{2E_1E_2(1-\cos\theta_{12})}$, where E_1, E_2 are the measured energies for the two largest clusters and θ_{12} is the opening angle between the corresponding tracks. Events with $m_{ee} < 2.0$ GeV/c^2 were rejected. About 96% (ϵ_{prelim}) of the events from reaction (2.2) survived this selection.

The first analysis method (hereafter referred to as the 'inclusive' selection) relied uniquely on the identification of 2 electrons reconstructing to the J/ψ mass. The criteria for the definition of an electron were derived by studying the characteristics of $\sim$ 4000 background-free events from the reaction:

$$\bar{p} + p \rightarrow J/\psi \rightarrow e^+ + e^- \tag{4.1}$$

collected in a scan at the J/ψ formation energy. Moreover, a sample of events collected in a control energy region (see Table 1), where no resonances were found, was useful for background studies. As expected, the background is dominated by Dalitz decays of the large π^0 component and by conversions of photons from π^0 decays, taking place predominantly in the 0.2 mm thick stainless steel vacuum pipe of the accumulator ring.

Four quantities were used to identify single electrons: the amplitude of the signals from the 4 mm thick H2 counters and from the Cherenkov counters, and the second moments in θ and ϕ of the energy clusters in the lead glass calorimeter. For each of the four variables, a probability density function for single electrons was obtained from the distribution of the $\sim$ 8000 electrons from reaction (4.1). Each electron candidate in the χ final states was then

assigned an 'electron quality index' defined as the product of the four probability densities computed at the measured values of the H2 and Cherenkov signal amplitudes and transverse shower moments. Background events are characterized by tracks with a low value of the 'electron quality index'. The selection of χ candidates was thus performed by requiring that the product of the 'electron quality index' for the two electron candidates be larger than a value chosen empirically to optimize the signal to background ratio and event acceptance. The efficiency of the cut was determined by applying the same selection criteria to the events from reaction (4.1).

Distributions of the reconstructed mass, m_{ee}, are shown in Figure 2. The open area in figure 2a refers to the events collected in the χ_2 scans which pass the preliminary cuts. The shaded area corresponds to events collected outside the resonance, in the control region, and normalized to an equivalent luminosity. A large low mass background is present in this sample which is seen to diminish considerably when the combined cut on the 'electron quality index' is applied (Figure 2b). For comparison, we give in Figure 2c the corresponding distribution for the event sample from reaction (4.1). The efficiency of the electron quality cut is $(85.6 \pm 0.7)\%$. A further cut accepting only events with $m_{ee} > 2.75$ GeV/c^2, reduced the efficiency to $(83.3 \pm 0.7)\%$. The results of this analysis are summarized in Table 2 where background levels are also given.

In the second method of analysis (the 'exclusive' selection), kinematical fits to reaction (2.2) were performed on all events which survived the preliminary cuts. They included: a) events where the γ in the final state fell within the acceptance of the calorimeters and was detected and b) events where the photon escaped detection (less than 20% of the entire sample). Energy and momentum conservation and the condition that the e^+e^- come from J/ψ decay provide five constraints for type 'a' events and two for type 'b' events which were treated by the method of Lagrange multipliers in the χ^2 minimization process. An event was accepted if the probability of the fit was greater than 10^{-4}. The actual efficiency of the selection was determined by applying this fit procedure to an almost background free

χ sample obtained with a restrictive cut on the 'electron quality index' of the two charged particles, and found to be (90.6±1.1)%. In Table 2 we compare the results of the two analyses. The two selections, based on independent cuts, yield statistically consistent samples.

The final sample is obtained by requiring that events accepted by the exclusive selection have the identity of at least one of the two electron candidates confirmed by a high value of the electron quality index. The efficiency of this selection was $\epsilon_{cuts} = (89.3 \pm 1.3)\%$. Figure 2d shows the distribution of m_{ee} for these events. The shaded area is, again, the residual background.

5. Analysis and Results

The data from each scan were subdivided into groups of events corresponding to a nominal value of the beam energy. Within a step, the central value of the energy could drift and the width of the momentum spectrum could change due to energy loss in traversing the hydrogen jet and energy changes caused by the momentum stochastic cooling. To monitor these effects, the beam frequency spectrum was measured and recorded every three minutes. The transverse position of the beam at 48 measuring stations around the ring was also recorded to check the stability of the beam orbit.

The resonance parameters were determined by a fit using a maximum likelihood technique. The likelihood function to be maximized, L, is written as the product of N (= number of data points in the excitation curve) Poisson functions, each giving, for the j-th data point, the probability that n_j events be observed if ν_j are expected:

$$L = \prod_{j=1,N} \frac{\nu_j^{n_j} e^{-\nu_j}}{n_j\,!}. \tag{5.1}$$

where:

$$\nu_j = \left[\int \mathcal{L}\, dt\right]_j \left(\sigma_{bckg} + \epsilon \int dW\, f_j(W) \sigma_{peak} \frac{\Gamma_R^2}{4\,(W - M_R c^2)^2 + \Gamma_R^2}\right) \tag{5.2}$$

The integral gives the convolution of the resonance Breit-Wigner with the center of mass energy distribution function $f_j(W)$, $\int \mathcal{L}\, dt$ is the integrated luminosity for each step, σ_{bckg} is the background cross section, ϵ is an overall acceptance–efficiency factor and:

$$\sigma_{peak} = \frac{4\pi(\hbar c)^2(2J_R+1)}{W^2 - 4m^2c^4} \times BR(R \to \bar{p}p) \times BR(R \to J/\psi\gamma) \times BR(J/\psi \to e^+e^-). \quad (5.3)$$

The parameters fitted were M_R, Γ_R and the product:

$$\Gamma(R \to \bar{p}p) \times BR(R \to J/\psi\gamma) \times BR(J/\psi \to e^+e^-) \quad (5.4)$$

which is proportional to the measured area under the excitation curve and therefore depends only on our knowledge of ϵ and $\int \mathcal{L}\, dt$ and not on the characteristics of the beam. All other quantities in (5.2) were input to the fit. The uncertainties on these quantities were used to estimate the systematic errors.

The integrated luminosity for each step, $\int \mathcal{L}\, dt$, was obtained by processing the pulse height spectrum from the silicon detector located at 86.5^0 to the beam direction (Figure 3). This involved the subtraction of a low level background under the proton peak (the dominant feature in Figure 3) and a correction for dead time in the data acquisition. We estimate a point-to-point uncertainty of 3% in the calculated luminosity and an overall scale error of 4% due to the uncertainty in the value of the $\bar{p}p$ elastic cross section[16] and in the detector acceptance.

The background cross section, σ_{bckg}, was measured at the control region and found to be 22 ± 3 pb^{-1}.

The overall efficiency–acceptance, ϵ, is the product of three factors: α_{geom}, the geometrical acceptance for $e^{\pm}$ in the fiducial volume ($15^0 < \theta < 60^0$), ϵ_{trig}, the efficiency of the trigger elements and ϵ_{anal}, the efficiency of the cuts performed at the analysis level . The value of α_{geom} depends on the shape of the angular distribution of the e^+e^- in the final state. To calculate the geometrical acceptance it was therefore necessary to fit the measured angular distribution to the expected functional form[17] which can be written in terms of

two parameters, the first one depending on the relative helicity amplitudes in the formation process and the second describing the multipole structure of the radiative decay† This procedure yielded $\alpha_{geom} = (62 \pm 1)\%$ for the χ_1 and $\alpha_{geom} = (62 \pm 2)\%$ for the χ_2 state. The trigger efficiency, ϵ_{trig}, was $(83 \pm 3)\%$. The dominant loss was in the charged particle defining coincidence between H1, H2 and the Cherenkov counter elements which did not allow for overlaps between adjacent octants and therefore missed a fraction of the particles due to the fact that the source was not a point. Finally, with the value of ϵ_{anal} for the final sample, $\epsilon_{anal} = \epsilon_{prelim} \times \epsilon_{cuts} = (86 \pm 2)\%$ we obtained:

$$\epsilon = \alpha_{geom} \times \epsilon_{trig} \times \epsilon_{anal} = (44 \pm 2)\% \text{ for both } \chi_1 \text{ and } \chi_2.$$

The center of mass energy spectrum for the j-th point, $f_j(W)$, was obtained with a transformation of variables from the beam momentum spectrum. As noted in Section 2, the beam momentum distribution can be derived from the measured revolution frequency spectrum and the machine parameter η. This spectrum could be accurately fit by the sum of two half gaussians joined at the peak (Figure 4), with the low momentum (high frequency) side on average $\sim 20\%$ wider than the high momentum side. For each reading, the frequency spectrum could then be parametrized by the frequency (f_r^0) corresponding to the peak of the distribution and by the widths of the two half gaussians $\left(\sigma_{f_r}^l \text{ and } \sigma_{f_r}^h\right)$.

The average over all spectrum readings was used for each energy step. The value for the beam momentum at the peak of the distribution,

$$p^0 = mc\beta\gamma = mc\left(f_r^0 L_{orb}/c\right) / \sqrt{\left(1 - (f_r^0 L_{orb}/c)^2\right)}, \tag{5.5}$$

can be obtained if the length of the orbit, L_{orb}, is known. $L_{orb} = L_0 + \delta L$ where L_0 is a reference orbit length [4] and δL is the deviation from this reference orbit. The reference orbit length is determined to ± 0.7 mm from the study of the ψ' excitation curve and δL

†In the case of χ_1 formation, only the helicity 1 state of $\bar{p}p$ is allowed by the rules of angular momentum composition and therefore the angular distribution depends only on one parameter.

is measured with a precision of ± 1 mm from the readings of the 48 position monitoring stations[4] The uncertainty in L_0 affects only the measurement of the mass of the resonance. At the χ's formation energy an error of ± 0.7 mm gives $\Delta M_R = \pm 80$ keV/c^2. The errors in δL may locally distort the excitation curve affecting also the measurement of the resonance width.

Figures 5a and 5b show the measured cross section for process (2.2) versus the center of mass energy for χ_1 and χ_2, respectively. A typical center of mass energy distribution is shown for comparison (dashed curves). The full line represents the best fit to the data. The results of the fits are given in Table 3 and Table 4 respectively for the χ_1 and for the χ_2. For each resonance, two scans were performed at different times and with machine tunes having different values of the parameter η. We have first fit the data of these scans separately ('a' and 'b'). Since for both resonances we found compatible sets of results, we have performed the final fits summing over the data from the two scans ('c' and figures 5) To check the stability of the results versus event selection criteria we have repeated the fits on the samples derived with the two independent methods described in Section 4. In Table 3 and 4, 'd' refers to the 'inclusive' and 'e' to the 'exclusive' selection samples. The final results are summarized in Table 5.

The systematic error on $\Gamma(R \to \bar{p}p) \times BR(R \to J/\psi\gamma) \times BR(J/\psi \to e^+e^-)$ has been computed by varying the values of $\epsilon, [\mathcal{L}dt]_j$ and σ_{bckg} one at a time, by a quantity equal to their estimated r.m.s. error and combining in quadrature the resulting shifts. When computing the systematic error on the total width Γ_R we have also included the errors on the parameters which characterize the beam energy spectrum ‡ Only the uncertainty in the orbit length contributes to the systematic error in the mass.

The partial widths $\Gamma(R \to \bar{p}p)$ were obtained from the value of $[\Gamma(R \to \bar{p}p) \times BR(R \to$

‡We call systematic all the errors not depending on event statistics even if some of the contributions are associated to random variables.

$J/\psi\gamma) \times BR(J/\psi \to e^+e^-)]$, using the published values[5] § for $BR(R \to J/\psi\gamma) \times BR(J/\psi \to e^+e^-) = (1.88 \pm 0.27)\%$ at the χ_1 and $(0.93 \pm 0.14)\%$ at the χ_2. The first error given on $\Gamma(R \to \bar{p}p)$ is from the uncertainty in our measurement ¶ while the second derives from the uncertainty in the branching ratios. Finally, we have obtained $BR(R \to \bar{p}p)$ from the ratio of the partial width $\Gamma(R \to \bar{p}p)$ to the total width, using the correlation matrix between the two quantities to estimate the errors.

These results represent a substantial improvement over previous data. The mass measurements agree with the existing ones[5] and the errors are reduced by factors of more than two. The improvement in the knowledge of total widths is even more substantial: we have a measurement of Γ_{χ_1} to $\pm 20\%$ whereas previously only an upper limit (< 1.3 MeV with 95% C.L.) was available; we obtain an error of 10% in Γ_{χ_2} which was known before this experiment to $\sim 40\%$. The error on the partial widths, $\Gamma(\chi \to \bar{p}p)$, has also been reduced and, for the first time, we obtain a precise measurement of the $BR(\chi_1 \to \bar{p}p)$.

6. Comparison with theoretical predictions

a. Hadronic Widths

Predictions for the hadronic widths of the χ states have been calculated to the lowest order and, for χ_0 and χ_2, first order corrections (in square brackets below) have been estimated[19,20]:

$$\Gamma(\chi_0 \to gg) \simeq \left(6\alpha_s^2 \mid R'_p(0) \mid^2 / m_c^4\right) \times (1 + [9.5\alpha_s/\pi]) \tag{6.1}$$

$$\Gamma(\chi_1 \to q\bar{q}g) \simeq \left(\frac{8}{9\pi} n_f \, \alpha_s^3 \mid R'_p(0) \mid^2 / m_c^4\right) \times ln(m_c < r >) \tag{6.2}$$

$$\Gamma(\chi_2 \to gg) \simeq \left(\frac{8}{5}\alpha_s^2 \mid R'_p(0) \mid^2 / m_c^4\right) \times (1 - [2.2\alpha_s/\pi]) \tag{6.3}$$

§ A recent measurement [18] gives a lower value for $BR(J/\psi \to e^+e^-)$.

¶ Statistical and systematic errors are combined in quadrature.

where $\alpha_s \equiv \alpha_s(m_c)$ is the running coupling 'constant' of the strong interactions calculated at the c-quark mass value $m_c = 1.5$ GeV/c^2 , $n_f = 3$ is the number of light flavors, $< r >= 3.17$ GeV^{-1} is the confinement radius and $\mid R'_p(0) \mid$ is the first derivative of the radial wave function at the origin for the $(c\bar{c})$ system in a P-state ‖.

$\mid R'_p(0) \mid$ has been estimated by solving a Schrodinger equation with a phenomenological central potential; its numerical value depends rather strongly on the functional shape of the potential[21]. The hadronic widths can be written as:

$$\Gamma_{had} \simeq \Gamma_R - \Gamma_R(\chi \to J/\psi\gamma) = \Gamma_R(1 - BR(\chi \to J/\psi\gamma)).$$

Inserting the known values[5] of the branching ratios for radiative decays we obtained from our measurements:

$$\Gamma_{had} = (0.64 \pm 0.11) \text{ MeV for } \chi_1 \text{ and } \Gamma_{had} = (1.71 \pm 0.21) \text{ MeV for } \chi_2.$$

In addition, we take from the literature [22] : $\Gamma(\chi_0 \to gg) \simeq \Gamma_{\chi_0} = 13.5 \pm 5.3$ MeV.

To lowest order, the ratio between $\Gamma(\chi_0 \to gg)$ and $\Gamma(\chi_2 \to gg)$ is independent of the wave function of the $(c\bar{c})$ state and of the value of α_s, $\Gamma(\chi_0 \to gg)/\Gamma(\chi_2 \to gg) = 15/4$. When first order radiative corrections are included, using for α_s the value [20] $0.276 \pm .014$ we obtain from equation (6.1) and (6.3):

$$\Gamma(\chi_0 \to gg)/\Gamma(\chi_2 \to gg) = \frac{15}{4} \times (2.27 \pm 0.08) = 8.53 \pm 0.30$$

which should be compared to the experimental value of 7.9 ± 3.9, where the large error comes from the uncertainty on Γ_{χ_0}

If we use the quoted value of α_s, we estimate from the value of $\Gamma(\chi_2 \to gg)$

‖While using equations (6.1), (6.2) and (6.3) as a guideline, we are aware of the fact that the prescription to calculate radiative corrections is not unique and that the magnitude of first order corrections, for charmonium, is such as to cast doubts on the convergence of the perturbative series.

$|R'_p(0)|^2 = 0.088 \pm 0.012$ GeV^5.

This should be compared to the theoretical predictions[21] which vary from 0.057 to 0.11 GeV^5 , depending on the functional form of the potential.

It is also interesting to compare our measurement for the $\Gamma(\chi_1 \to q\bar{q}g)$ with the theoretical calculation which, in this case, stops at the lowest order (Eq. 6.2). Using again the same value for α_s and for $|R'_p(0)|^2$ the value derived from the $\Gamma(\chi_2 \to gg)$, we obtain $\Gamma(\chi_1 \to q\bar{q}g) \sim 0.50$ MeV to be compared with the experimental value of (0.64 ± 0.11) MeV.

b. Radiative widths.

Precise estimates of the widths for electric dipole $P \to S$ transitions can be obtained by combining the known branching ratios[5] and our measured values for the total widths of χ_1 and χ_2. These widths, given in Table 6, are at the low end of theoretical predictions[23–25] The relative magnitude of the two partial widths is compatible with the expected E_γ^3 scaling law.

c. Partial widths to $\bar{p}p$.

Large momentum transfer exclusive reactions can be analyzed in the framework of QCD with the application of a factorization theorem [26] which separates the dynamics of the hard–scattering quark–gluon amplitudes (T_h) from process independent quark distribution amplitudes. At sufficiently large values of Q^2, T_h can be evaluated perturbatively. For the decays of $(\bar{c}c)$, where $Q^2 \sim 10$ GeV^2, this technique should give reliable results.

A simple application is that of calculating the relative magnitude of branching ratios to a $\bar{p}p$ final state from different $(\bar{c}c)$ states. In this way, estimates of the branching ratio $BR(\chi_2 \to \bar{p}p)$ have been obtained by several authors [27,28,29], using a normalization of the $p(\bar{p})$ quark (antiquark) distribution amplitudes extracted from the analysis of $J/\psi \to \bar{p}p$ [30]. It is found [27] that $BR(\chi_2 \to \bar{p}p)$ is relatively insensitive to variation of the form of the quark distribution amplitudes. Predicted values of the branching ratio for the χ_2 are given in Table

7, and show, in general, satisfactory agreement with the experimental results reported here.

7. Summary

Fermilab experiment E760 has recorded its first data in the summer 1990. During that period, we performed energy scans at the χ_1 and χ_2 resonances and obtained precise measurements of mass, total width and partial width to $\bar{p}p$ for both states. In particular, for the first time, the total width of the χ_1 state was determined. The direct measurement of widths in the sub–MeV region is made possible in our experiment by the excellent definition of the energy of the initial $\bar{p}p$ state. Compilation of results is given in Table 5.

Our results on total hadronic widths, radiative widths for $\chi_{1,2} \rightarrow J/\psi\gamma$ and partial widths to $\bar{p}p$ are in good agreement with theoretical predictions based on perturbative QCD.

8. Acknowledgements

The successful construction, integration and operation of the E760 detector was made possible by the dedicated technical support staffs from the collaborating institutions, whose superb effort we gratefully acknowledge. The crucial contribution of the Fermilab Accelerator Division Antiproton department is also gratefully acknowledged. This work was funded by the U.S. Department of Energy and the National Science Foundation and by the Italian Istituto Nazionale di Fisica Nucleare.

References

[1] C. Baglin, *et al.*, Nucl. Phys. **B286**, (1987) 592.

[2] J. Peoples Jr., " Prospects for $\bar{p}p$ experiments in the TeV I accumulator", p. 144, Low Energy Antimatter, Workshop on the Design of a Low Energy Antimatter Facility, October 1985, ed. D. Cline, World Scientific Publishing Co. 1986.

V. Bharadwaj, *et al.*, " Operation of the Fermilab Accumulator Medium Energy Proton-Antiproton Physics", p. 617, EPAC 90, Proceedings of the 2^{nd} European Particle Accelerator Conference, 1990, eds. P. Marin and P. Mandrillon, Editions Frontieres, Gif-sur-Yvette, Cedex, France, 1990.

[3] W. Kwong, C. Quigg and L. Rosner, Ann. Rev. Nucl. Part. Sci. **37** (1987) 325.

[4] T.A. Armstrong, *et al.*., " Precision measurements of Charmonium States in the Fermilab Accumulator", to be submitted for publication to Physical Review D.

[5] Review of Particle Properties, Particle Data Group, Phys. Lett. **B239**, (1990) 1 and references therein.

[6] M. Macrí', " Gas Jet Targets", CERN Accelerator School 1983, CERN 85-15 (1985)

[7] M. Sarmiento, *et al.*, " A Luminosity Monitor for FNAL Experiment E760 ", to be submitted for publication to Nucl. Instr. and Meth.

[8] C. Biino, *et al.*, Nucl. Instr. and Meth. **A271**, (1988) 417; C. Biino, *et al.*, IEEE Trans. on Nucl. Sci. **36** (1989) 98.

[9] R. Calabrese, *et al.*, Nucl. Instr. and Meth. **A277**, (1989) 116; R. Calabrese, *et al.*, IEEE Trans. on Nucl. Sci. **36**, (1989) 54.

[10] C. Biino, *et al.*, " A Large Acceptance Threshold Cherenkov Counter for Experiment E760 at Fermilab", to be submitted for publication to Nucl. Instr. and Meth.

[11] G. Barisone, *et al.*, INFN/AE - 89/6 (1989).

[12] L. Bartoszek, *et al.*, Nucl. Instr. and Meth. **A301**, (1991) 47.

[13] M.A. Hasan, *et al.*, Nucl. Instr. and Meth. **A295**, (1990) 73.

[14] S. Hansen, *et al.*, IEEE Trans. on Nucl. Sci. **34**, (1987) 1003.

[15] I. Gaines, *et al.*, Computer Physics Communications **45**, (1987) 323; C. Gay, *et al.*, IEEE Trans. on Nucl. Sci. **34**, (1987) 870.

[16] M.M. Block and R.N. Cahn, Review of Modern Physics **57**, No.2, (1985).

[17] A.D. Martin, M.G. Olsson and W.J. Stirling, Phys. Lett. **147B**, (1984) 203.

[18] D. Coffman, *et al.*,"A Direct Measurement of the J/ψ Leptonic Branching Fraction", SLAC-PUB-5592, submitted to Phys. Rev. Lett.

[19] R. Barbieri, M. Caffo, R. Gatto and E. Remiddi, Nucl. Phys. **B192**, (1981) 61.

[20] W. Kwong, P.B. Mackenzie, R. Rosenfeld and J.L. Rosner, Phys. Rev. D **37**, (1988) 3210.

[21] M.G. Olsson, A.D. Martin and A.W. Peacock, Phys. Rev. D **31**, (1985) 81.

[22] J.E. Gaiser, *et al.*, Phys. Rev. D **34**, (1986) 711.

[23] E. Eichten,*et al.*, Phys. Rev. D **21**, (1980) 203.

[24] R. McGlary and N. Byers, Phys. Rev. D **28**, (1983) 1692.

[25] S.N. Gupta, W.W Repko and C.J. Suchyta III, Phys. Rev. D **39**, (1989) 974.

[26] A. Duncan and A.H. Mueller, Phys. Rev. D **21**, (1980) 1636; S.J. Brodsky and G.P. Lepage, Phys. Rev. D **22**, (1980) 2157.

[27] E.L. Berger, P.H. Damgaard and K. Tsokos, "QCD Predictions for Charmonium Production in $p\bar{p}$ Collisions" in Proceedings of the VIIth European Symposium on Antiproton Interactions, Durham, UK, July 9 -13, 1984, p. 349.

[28] V.L. Chernyak and I.R. Zhitnitsky, Nucl. Phys. B **246**, (1984) 52.

[29] A. Andrikopoulou, Z. Phys. C **22**, (1984) 63.

[30] S.J. Brodsky and G.P. Lepage, Phys. Rev. D **24**, (1981) 2848.

Table 1: Summary of the data recorded during the 1990 run

Resonance	P_{beam} (MeV/c)	Integrated Luminosity (nb^{-1})
J/ψ	4063.	360
ψ'	6232.	1470
χ_1	5550.	1030
χ_2	5724.	1160
Background	5660.	420
Background	~5605.	1250
Background	6110.	185

Table 2: Characteristics of the selected event samples

	INCLUSIVE SELECTION			EXCLUSIVE SELECTION			FINAL SAMPLE		
	No. of Events	Effic. %	Backg. Events	No. of Events	Effic. %	Backg. Events	No. of Events	Effic. %	Backg. Events
χ_1	498	83.3±0.7	25±4	538	90.6±1.1	44±5	513	89.3± 1.3	23±4
χ_2	554		29±4	617		49±6	585		26±4

Table 3: χ_1 Parameters

	M_{χ_1} (MeV/c^2)	Γ_{χ_1} (MeV)	$\Gamma_{\bar{p}p}BR^{**}_{fin}$ (eV)	No. of Events	χ^2/d.o.f.
a	$3510.439\ ^{+.060}_{-.062}$	$.98\ ^{+.19}_{-.16}$	$1.42\ ^{+.14}_{-.13}$	265	1.0
b	$3510.584\ ^{+.050}_{-.049}$	$.84\ ^{+.13}_{-.11}$	$1.21\ ^{+.11}_{-.10}$	248	1.3
c	$3510.531\ ^{+.037}_{-.037}$	$.88\ ^{+.11}_{-.10}$	$1.29\ ^{+.09}_{-.08}$	513	1.3
d*	$3510.539\ ^{+.037}_{-.037}$	$.88\ ^{+.11}_{-.10}$	$1.33\ ^{+.09}_{-.08}$	498	1.2
e	$3510.542\ ^{+.038}_{-.038}$	$.88\ ^{+.11}_{-.10}$	$1.29\ ^{+.09}_{-.08}$	538	1.4

Table 4: χ_2 Parameters

	M_{χ_2}(MeV/c^2)	Γ_{χ_2} (MeV)	$\Gamma_{\bar{p}p}BR^{**}_{fin}$ (eV)	No. of Events	χ^2/d.o.f.
a	$3556.136\ ^{+.207}_{-.186}$	$1.84\ ^{+.31}_{-.30}$	$1.48\ ^{+.22}_{-.20}$	189	1.2
b	$3556.142\ ^{+.069}_{-.070}$	$1.96\ ^{+.23}_{-.19}$	$1.72\ ^{+.11}_{-.10}$	396	1.1
c	$3556.155\ ^{+.065}_{-.066}$	$1.98\ ^{+.17}_{-.16}$	$1.67\ ^{+.09}_{-.09}$	585	1.2
d*	$3556.225\ ^{+.067}_{-.067}$	$1.99\ ^{+.18}_{-.16}$	$1.70\ ^{+.10}_{-.10}$	554	1.3
e	$3556.121\ ^{+.065}_{-.065}$	$1.92\ ^{+.17}_{-.15}$	$1.65\ ^{+.09}_{-.09}$	617	1.1

* It should be noted that any decay channel $\chi \rightarrow J/\psi + X$, where X is not a photon, would contribute to the 'inclusive' sample 'd' but not to the exclusive samples 'c' and 'e'.

** $BR_{fin} = BR(R \rightarrow J/\psi\gamma) \times BR(J/\psi \rightarrow e^+e^-)$

Table 5: Final results

Parameters	χ_1	χ_2
M_R (MeV/c^2)	$3510.53 \pm .04 \pm .12$	$3556.15 \pm .07 \pm .12$
Γ_R (MeV)	$0.88 \pm .11 \pm .08$	$1.98 \pm .17 \pm .07$
$\Gamma(R \to \bar{p}p)BR(R \to J/\psi\gamma)BR(J/\psi \to e^+e^-)$ (eV)	$1.29 \pm .09 \pm .13$	$1.67 \pm .09 \pm .12$
$\Gamma(R \to \bar{p}p)$ (eV)	$69 \pm 9 \pm 10$	$180 \pm 16 \pm 26$
$BR(R \to \bar{p}p)$	$(0.78 \pm .15) \times 10^{-4}$	$(0.91 \pm .15) \times 10^{-4}$

For the measured quantities, M_R, Γ_R and $\Gamma(R \to \bar{p}p)BR(R \to J/\psi\gamma)BR(J/\psi \to e^+e^-)$, the first errors quoted are statistical and the second are systematic.

Table 6: Radiative transition widths (keV) of χ_1 and χ_2

	Γ_γ^{exp}	$(\Gamma_\gamma^{exp}/E_\gamma^3) \times 10^9$ (MeV^{-2})
χ_1	240 ± 40	$4.08 \pm .70$
χ_2	267 ± 33	$3.36 \pm .42$

Table 7: BR($\chi \to \bar{p}p$) for χ_1 and χ_2 in unit of 10^{-4}

	experiment	Ref. 28	Ref. 29	Ref. 30
χ_1	0.75 ± 0.15	—	—	—
χ_2	0.87 ± 0.15	0.8 – 1.2	$\sim 1.$	2.0 – 2.1

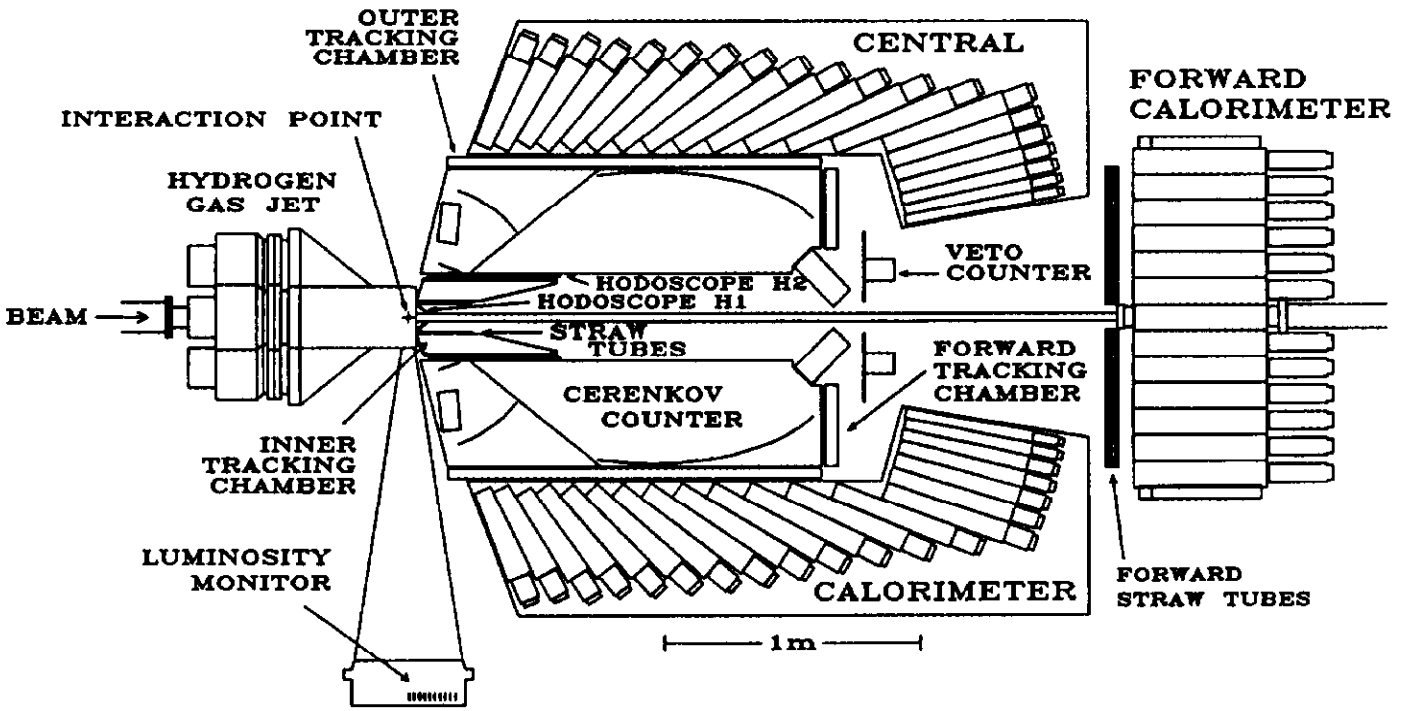

Fig. 1: E760 equipment layout.

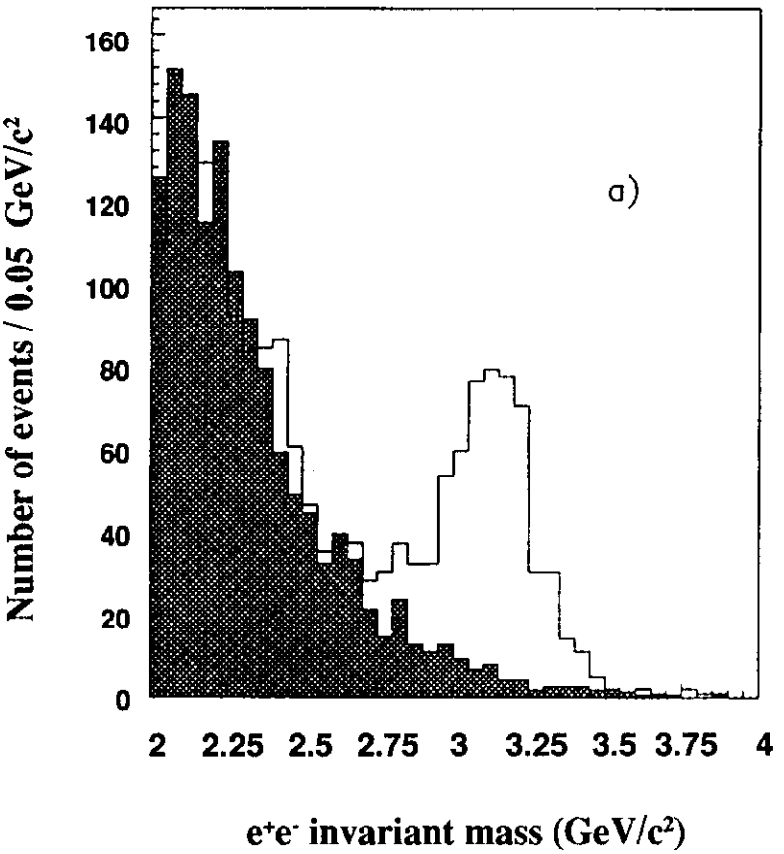

Fig. 2a: Distribution of the reconstructed e^+e^- invariant mass for the χ_2 sample passing preliminary cuts.

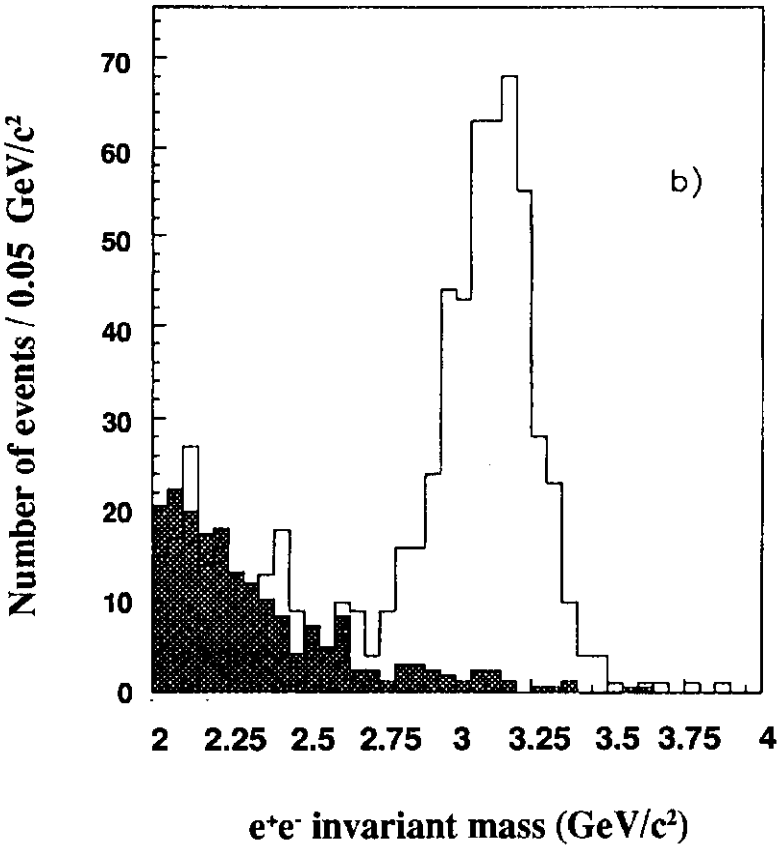

Fig. 2b: Distribution of the reconstructed e^+e^- invariant mass for the χ_2 sample after applying the cut on the electron quality index.

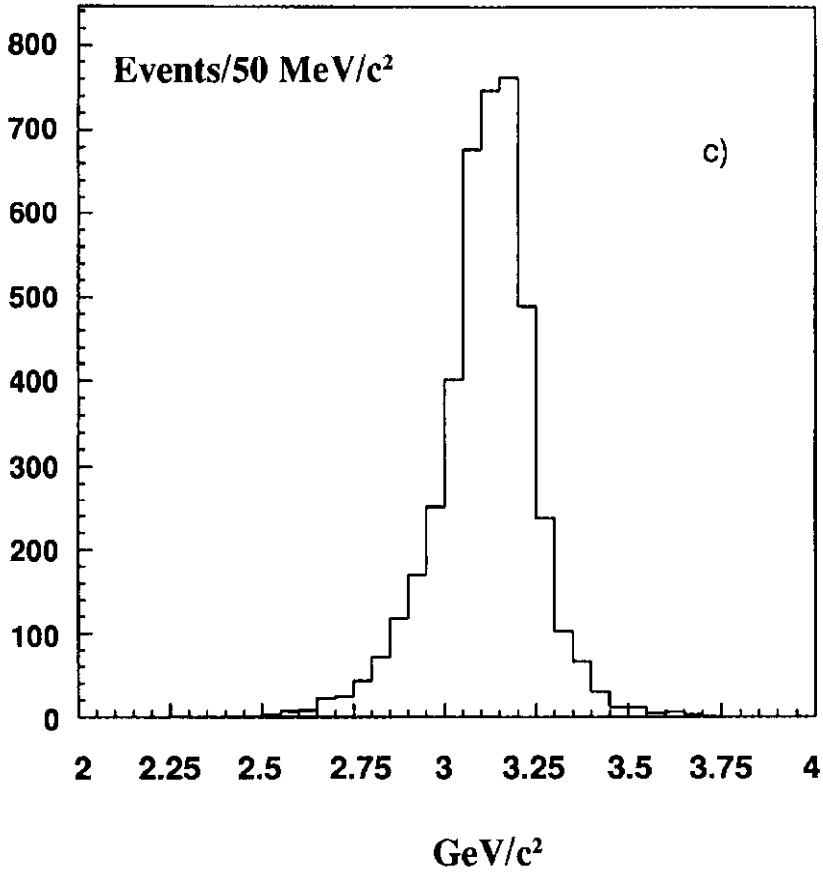

Fig. 2c: Distribution of the reconstructed e^+e^- invariant mass for a background-free event sample from reaction $\bar{p}p \rightarrow J/\psi \rightarrow e^+e^-$.

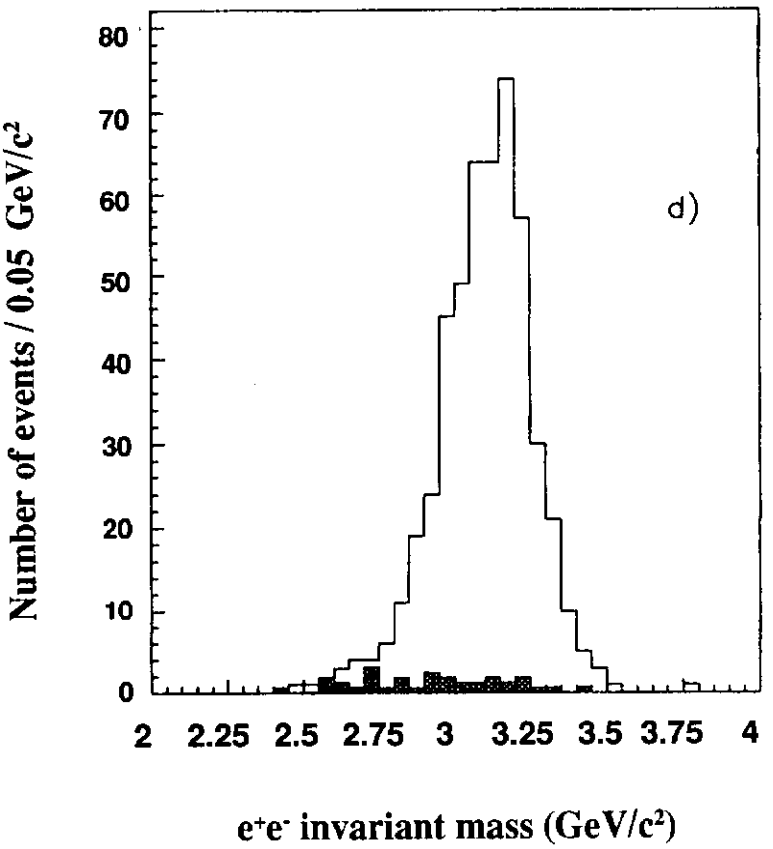

Fig. 2d: Distribution of the reconstructed e^+e^- invariant mass for the final χ_2 sample (see text).

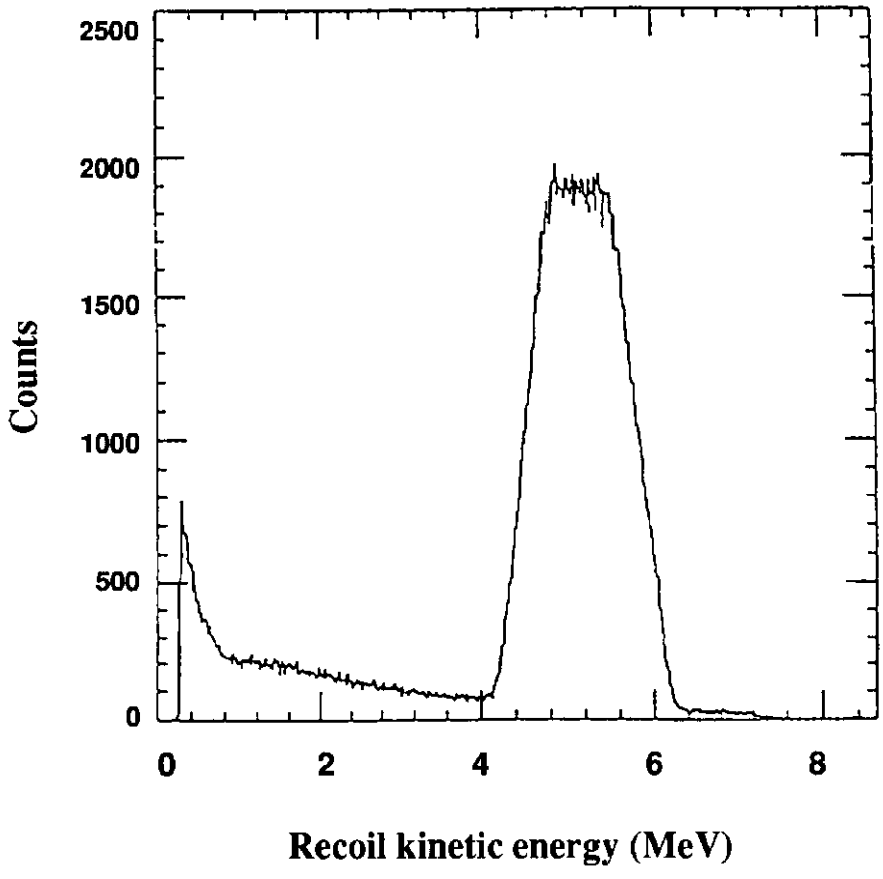

Fig. 3: Distribution of kinetic energy as measured by a silicon detector of the luminosity monitor.

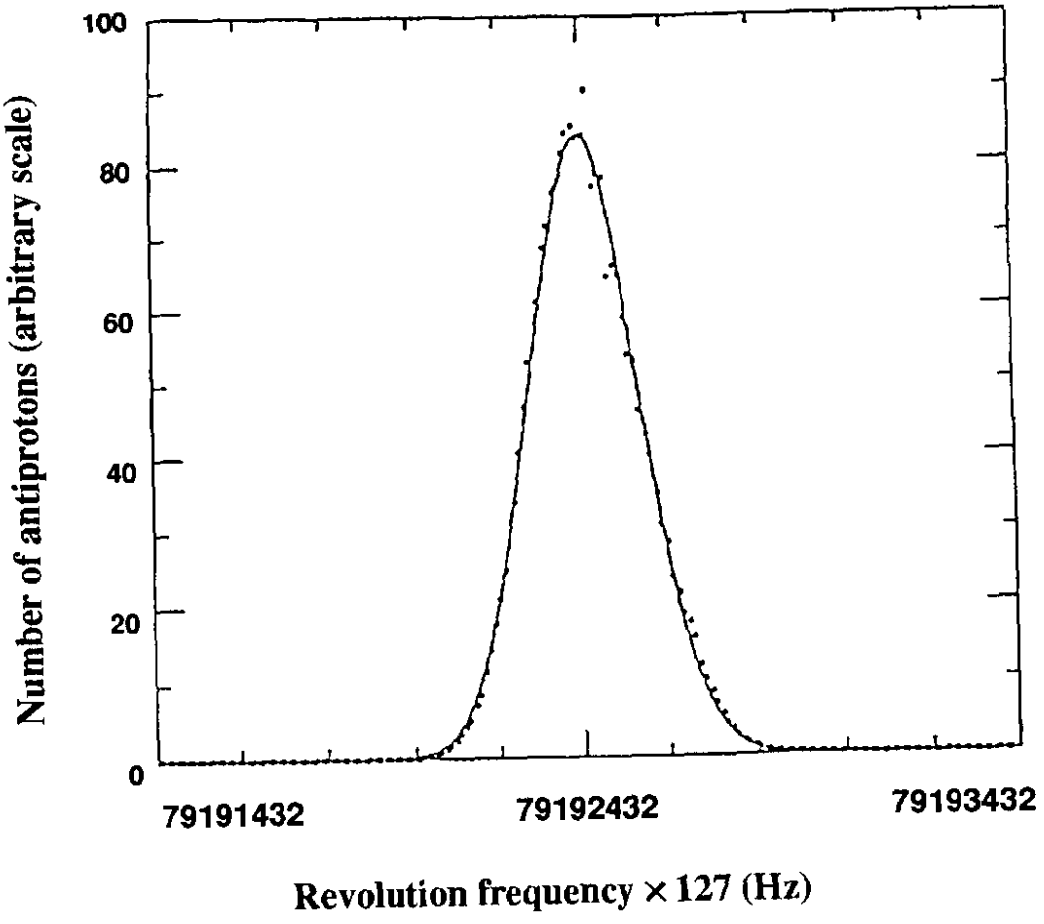

Fig. 4: The beam current Schottky noise spectrum at the 127th harmonic of the beam revolution frequency. The data points are the average over many measurements. The continuous line is the result of an asymmetric gaussian fit to the data points.

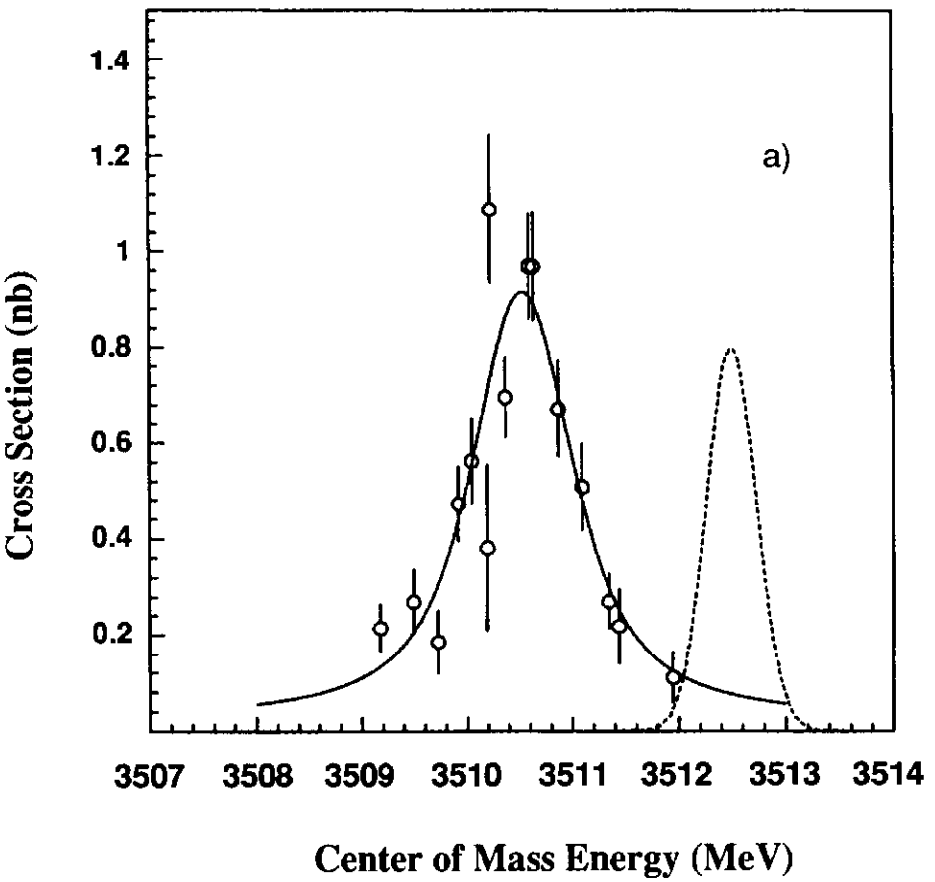

Fig. 5a: Measured cross section for the energy scan at the χ_1. Full line represents the best fit to the data. The dashed curve shows a typical center of mass energy distribution (arbitrary vertical units).

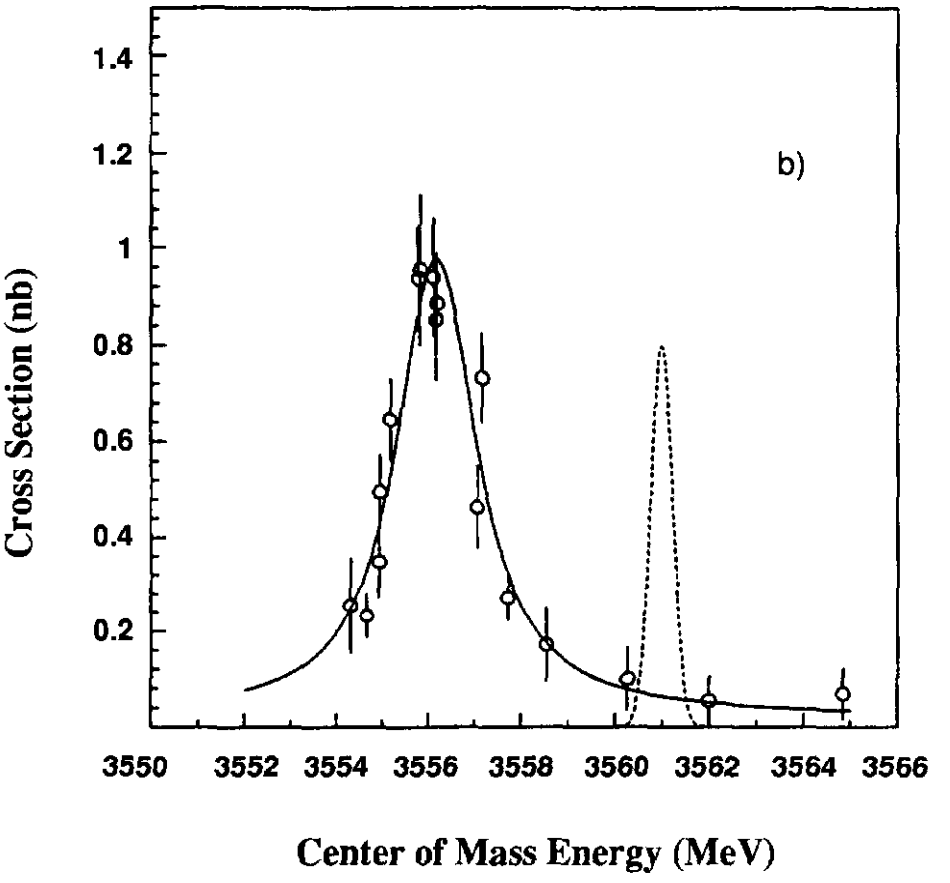

Fig. 5b: Measured cross section for the energy scan at the χ_2. Full line represents the best fit to the data. The dashed curve shows a typical center of mass energy distribution (arbitrary vertical units).